

**Synthesis, characterisation, experimental and electronic structure of novel
Dichloro(bis{2-[1-(4-methoxyphenyl)-1H-1,2,3-triazol-4-yl-kN3]pyridine-kN})metal(II)
compounds, metal = Mn, Co and Ni**

J. Conradie^{1*}, MM Conradie¹, K. Tawfiq², M. Al-Jeboori³, S.J. Coles⁴ and J.H. Potgieter^{2,5*}

1. Department of Chemistry, University of the Free State, P.O. Box 339, Bloemfontein, 9300, South Africa

2. Division of Chemistry and Environmental Science, Manchester Metropolitan University, Manchester, M1 5GD, UK

3. Department of Chemistry, University of Baghdad, Baghdad, Iraq

4. EPSRC National Crystallography Service, School of Chemistry, University of Southampton, Southampton, SO17 1BJ, England
5. School of Chemical and Metallurgical Engineering, University of the Witwatersrand, Private Bag X3, Wits, 2050, South Africa

*Contact author details:

Name: Jeanet Conradie

Tel: +27-51-4012194

Fax: +27-51-4017295

e-mail: conradj@ufs.ac.za

Abstract

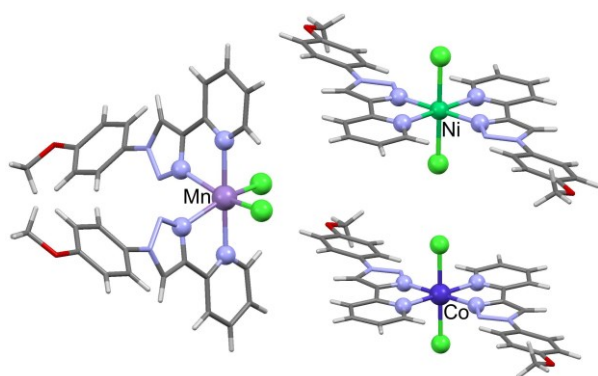
Three syntheses, characterizations and structures of three novel and dichloro(bis{2-[1-(4-methoxyphenyl)-1H-1,2,3-triazol-4-yl-kN3]pyridine-kN})metal(II) complexes (metal = Mn, Co and Ni) are presented and compared to the related iron(II) structure. In the solid state the molecules are arranged in infinite hydrogen-bonded 3D supramolecular chains, further stabilized by with weak intermolecular $\pi \dots \pi$ interactions. DFT results all the different spin states and isomers of dichloro(bis{2-[1-phenyl-1H-1,2,3-triazol-4-yl-kN3]pyridine-kN})metal(II) complexes, $[M(L^1)_2Cl_2]$, support experimental measurements, namely that (i) d^5 $[Mn(L^1)_2Cl_2]$ is high spin with $S = 5/2$; (ii) d^6 $[Fe(L^1)_2Cl_2]$ is high spin with $S = 2$; (iii) d^7 $[Co(L^1)_2Cl_2]$ has a spin state of $S = 3/2$; (iv) d^8 $[Ni(L^1)_2Cl_2]$ has a spin state of $S = 1$; and (v)

for all $[M(L^1)_2Cl_2]$ complexes, the *cis-cis-trans* and the *trans-trans-trans* isomers, with the pyridyl groups *trans* to each other, have the lowest energy.

Keywords

(1,2,3-triazol-4-yl)pyridine; manganese; cobalt; nickel; DFT

TOC graphics and text



Structure of high spin *cis* and *trans* metal(II)-(1,2,3-triazol-4-yl)pyridine complexes metal = Mn, Fe, Co and Ni

Highlights

Structures of *cis* and *trans* metal(II)-(1,2,3-triazol-4-yl)pyridine complexes

H-bonded 3D supramolecular chains in solid state

High spin metal(II)-(1,2,3-triazol-4-yl)pyridine complexes

1 Introduction

There are many sources of energy alternative to conventional fossil fuels. One of these is the photovoltaic cell. Current commercial photovoltaic devices are most commonly silicon based solid state cells. The main aim in the development of photovoltaic cells is to achieve the highest possible efficiency, converting as much sunlight as possible to electrical energy,

whilst also keeping the cost to a minimum to ensure affordability for commercial use. One such development in this area is the Dye-sensitized solar cell (DSSC). DSSCs are the most efficient 3rd generation photovoltaic devices and were first proposed by Michael Grätzel in 1991 [1]. The DSSC has 5 main components, a semiconductor, transparent conducting layer, sensitized dye, electrolyte and a counter electrode. The process of energy conversion is triggered when the dye is exposed to sunlight. Being photosensitive, the dye molecule enters an excited state, promoting an electron from the HOMO to the LUMO. This results in the injection of the electron into the conduction band of the semiconductor and this oxidises the dye. The sensitized dye is then reduced and immediately regenerated when it accepts an electron from the redox couple in the electrolyte. The electrolyte is subsequently reduced by the counter electrode or cathode. This regeneration process allows the sustained conversion of light energy [2]. There are a number of criteria which the sensitized dye must fulfil in order to be deemed suitable for use in a DSSC. Firstly, it should be able to absorb all wavelengths of light below 920 nm. Secondly, there needs to be a good anchoring group present, allowing it to bind firmly and irreversibly, through the process of chemisorption, to the semiconductor. Also, if the electron density is centred on the anchoring group, there will be a more efficient electron injection to the semiconductor. With regards to energy levels, the LUMO of the dye should be above the conduction band edge of the semiconductor whilst the HOMO energy level should be below that of the redox electrode [3]. Ruthenium is the most commonly utilised metal in sensitized dyes [4,5]. DSSCs utilise extrinsic semiconductors which can be found as two types. Firstly there is an n-type semiconductor, the most popular choice which utilises wide band-gap metal oxides such as TiO₂ and ZnO₂. The second type, the p-type, makes use of metal oxides such as NiO. N-type semiconductors have a large electron concentration compared to p-type semiconductors. The most popular semiconductor used in DSSCs is TiO₂, because it provides the highest efficiencies [6]. There are a couple of key requirements which an electrolyte must fulfil to increase the efficiency in a DSSC. Firstly, fast dye regeneration and secondly, slow electron recapture are essential. The most commonly used electrolyte is tri-iodide (I³⁻)/ iodide (I⁻) due to it fulfilling the necessary criteria. However, there are a few disadvantages to using iodine based electrolytes, including the inability to absorb light of wavelengths other than blue. This causes a decrease in the short circuit photocurrent and thus reduces the power conversion efficiency of the cell [7].

Cobalt complexes have been shown to be quite suitable when used as a DSSC electrolyte. Yella et al [8] used a Co(II/III)tris(bipyridyl)-based electrolyte coupled with a zinc-porphyrin sensitized dye and managed to achieve a power conversion efficiency of 12.3%. Similarly, Yum et al [9] tested a few different Co(II/III)tris(bipyridyl)-based electrolytes and discovered that they had a very high open circuit voltage, whilst also maintaining a low short circuit current. When used in conjunction with an organic sensitized dye, they produced a power conversion efficiency of greater than 10%. By using a tris(1,2-diaminoethane)cobalt(II)/(III) electrolyte in a p-type cell, Powar et al. [10] managed to obtain power conversion efficiencies of 1.3% and a very high open circuit voltage of 709 mV. Whilst this is relatively high for a p-type cell, about 2.3 times greater than the previous best performing p-type DSSCs, it is still quite low compared to n-type cells. However, whilst not being sufficiently efficient on their own, p-type cells could possibly be used in conjunction with n-type compounds to give better performance.

Currently triazole based dyes have not been investigated. Here we present and compare the structure, chemical and electronic properties of a series of pyridyl-triazole based transition metal complexes, namely d^5 Mn(II), d^6 Fe(II), d^7 Co(II) and d^8 Ni(II), for potential use as a sensitized dye in DSSCs. We recently reported on a series eight of iron complexes [11] containing differently substituted 1,2,3-triazole chromophores [12]. We thus extend the series here to other first row transition metal(II) complexes, containing the 1,2,3-triazole chromophores 2-(1-(4-methoxy-phenyl)-1H-1,2,3-triazol-1-yl)pyridine (Figure 1).

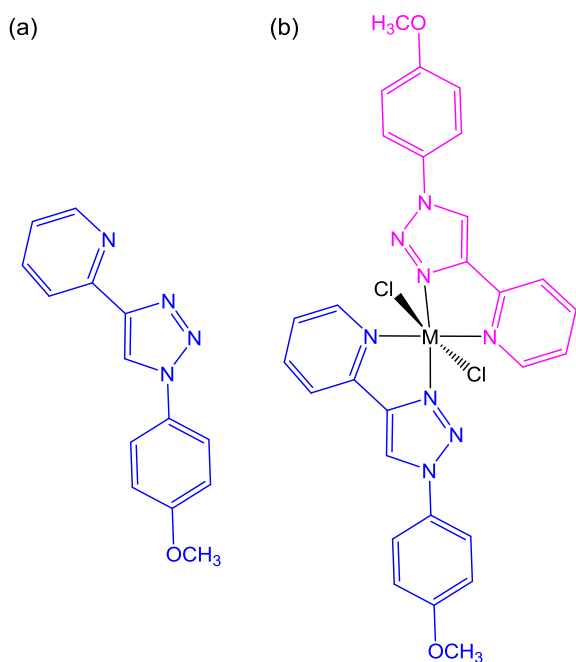


Figure 1: Structure of 2-(1-(4-methoxy-phenyl)-1H-1,2,3-triazol-1-yl)pyridine (L) and its metal(II) complex [ML₂Cl₂]. M = Mn, Fe, Co and Ni.

2 Methods and Materials

2.1 Synthesis of the 2-(1-(4-methoxy-phenyl)-1H-1,2,3-triazol-1-yl)pyridine-metal complexes [ML₂Cl₂]

The ligand, 2-(1-(4-methoxy-phenyl)-1H-1,2,3-triazol-1-yl)pyridine, was synthesized and characterized as described previously [13,14,15,16]. Standard literature methods were slightly adapted to synthesize the metal-pyridyl-triazole complexes. Generally 1 equivalent of the metal chloride and 2 equivalents of the 2-(1-(4-methoxy-phenyl)-1H-1,2,3-triazol-1-yl)pyridine ligand was stirred at room temperature (RT) for 8-10 h in a 1:1 mixture of CH₃OH and DCM as solvent. The solvent was removed under vacuum. The solid mass obtained was then washed with several volumes of cold methanol and diethyl ether [17].

2.1.1 Dichloro(bis{2-[1-(4-methoxyphenyl)-1H-1,2,3-triazol-4-yl-kN₃]pyridine-kN})Manganese(II)

The complex [Mn(L)₂Cl₂] was prepared by stirring a solution of anhydrous MnCl₂ (0.14g, 0.55 mmol) in CH₃OH (10 ml). A solution of the ligand L (0.03 g, 0.23 mmol, 2eq) in

CH₂Cl₂ (10 ml), was added dropwise to it. A resulting pale yellow precipitate was obtained after stirring for 8-10h at RT. The solvent was then reduced in volume by a half under vacuum distillation before it was filtered and washed twice with cold methanol and then diethyl ether. A pale, yellow solid was obtained and isolated to yield a precipitate that give the product (0.14 g, 0.22 mmol, yield 82%), mp. 310-312°C. IR: $\bar{\nu}$ (cm⁻¹): 3049, 3025, 2966, 2873, 1604, 1569, 1518, 1471, 1452, 1259, 1203, 1174, 1117, 1066, 1055, 1017, 1001, 980, 864, 827, 786, 751, 718. UV-Vis (DMSO) λ_{\max} : The Mn(II) complex showed absorption bands at 258 nm, $\epsilon_{\max} = 17780 \text{ dm}^3\text{mol}^{-1}\text{cm}^{-1}$, 291 nm, $\epsilon_{\max} = 19480 \text{ dm}^3\text{mol}^{-1}\text{cm}^{-1}$, 352 nm, $\epsilon_{\max} = 32 \text{ dm}^3\text{mol}^{-1}\text{cm}^{-1}$, 369 nm, $\epsilon_{\max} = 30 \text{ dm}^3\text{mol}^{-1}\text{cm}^{-1}$, 390 nm, $\epsilon_{\max} = 21 \text{ dm}^3\text{mol}^{-1}\text{cm}^{-1}$. $\mu_{\text{eff}} = 5.32$ B.M. HRMS TOF (ESI+) (water: acetonitrile = 1:3) with the highest molecular weight ion peak matching, was observed at $m/z = 594.1069$ (90%) and is attributed to [M-Cl]⁺. The calculated value for [(C₂₈H₂₄ClMnN₈O₂)]⁺ is 594.1091. A good single crystal for X-ray structural analysis was obtained by slow evaporation of a hot methanol solution of the complex. Λ_M (DMSO) = 52 $\Omega^{-1}\text{cm}^2\text{mol}^{-1}$.

2.1.2 Dichloro(bis{2-[1-(4-methoxyphenyl)-*l*H-1,2,3-triazol-4-yl-kN3]pyridine-kN})cobalt(II)

For the preparation of [CoL₂Cl₂], the method used was analogous to that for [MnL₂Cl₂]. An amount of CoCl₂.6H₂O of 0.045g, 0.16 mmol and 0.071 g, 0.32 mmol of L were used, and an identical work-up procedure gave the required compound as a pale pink solid, and the isolated precipitate gave (0.091 g, 0.14 mmol, yield 77%), mp. 340°C (decomp.). IR: $\bar{\nu}$ (cm⁻¹): 3068, 3052, 3030, 3014, 2966, 2839, 1609, 1597, 1574, 1518, 1471, 1453, 1320, 1261, 1204, 1175, 1067, 1058, 1019, 1003, 979, 860, 825, 786, 752, 720. UV-Vis (DMSO) λ_{\max} : The Co (II) complex showed absorption bands at 257 nm, $\epsilon_{\max} = 26625 \text{ dm}^3\text{mol}^{-1}\text{cm}^{-1}$, 292 nm, $\epsilon_{\max} = 11000 \text{ dm}^3\text{mol}^{-1}\text{cm}^{-1}$, 615 nm, $\epsilon_{\max} = 38 \text{ dm}^3\text{mol}^{-1}\text{cm}^{-1}$, 677 nm, $\epsilon_{\max} = 61 \text{ dm}^3\text{mol}^{-1}\text{cm}^{-1}$. $\mu_{\text{eff}} = 3.97$ B.M. HRMS TOF (ESI+) (water: acetonitrile = 1:3) with the highest molecular weight ion peak matching, was observed at $m/z = 598.1048$ (90%) and correspond to [M-Cl]⁺. The calculated value for [(C₂₈H₂₄ClCoN₈O₂)]⁺ is 598.1043. A good single crystal for X-ray structural analysis was obtained by slow evaporation of a hot DMSO: CH₃CN = 1:9 solution of the complex. Λ_M (DMSO) = 42 $\Omega^{-1}\text{cm}^2\text{mol}^{-1}$.

2.1.3 Dichloro(bis{2-[1-(4-methoxyphenyl)-1H-1,2,3-triazol-4-yl-kN3]pyridine-kN})nickel(II)

For the preparation of [NiL₂Cl₂], the method used was similar to that for [MnL₂Cl₂]. An amount of NiCl₂·6H₂O of 0.037 g, 0.15 mmol and 0.08 g, 0.31 mmol of L were used, and an identical work-up procedure gave the required compound as a pale blue solid. The isolated precipitate gave (0.073 g, 0.11 mmol, yield 74%), mp. 345°C (decomp.). IR: $\bar{\nu}$ (cm⁻¹); 3073, 3052, 3030, 2985, 2839, 1612, 1597, 1575, 1519, 1473, 1455, 1322, 1263, 1176, 1070, 1060, 1020, 1005, 980, 862, 825, 787, 754, 721. UV-Vis (DMSO) λ_{max} : The Ni (II) complex showed absorption bands at 257 nm, $\epsilon_{\text{max}} = 3602 \text{ dm}^3 \text{ mol}^{-1} \text{ cm}^{-1}$, 291 nm, $\epsilon_{\text{max}} = 3653 \text{ dm}^3 \text{ mol}^{-1} \text{ cm}^{-1}$, 407 nm, $\epsilon_{\text{max}} = 61 \text{ dm}^3 \text{ mol}^{-1} \text{ cm}^{-1}$, 660 nm, $\epsilon_{\text{max}} = 43 \text{ dm}^3 \text{ mol}^{-1} \text{ cm}^{-1}$. $\mu_{\text{eff}} = 2.73 \text{ B.M.}$ HRMS TOF (ESI+) (water: acetonitrile = 1:3) with the highest molecular weight ion peak matching, was observed at $m/z = 597.1086$ (80%) and is related to [M-Cl]⁺. The calculated value for [(C₂₈H₂₄ClNiN₈O₂)]⁺ is 597.1064. A good single crystal for X-ray structural analysis was obtained by slow evaporation of a hot DMSO: Acetonitrile = 1:9 solution of the complex. Λ_{M} (DMSO) = 54 $\Omega^{-1} \text{ cm}^2 \text{ mol}^{-1}$.

2.2 Instrumental conditions

Infrared (ATR-FTIR IR) spectra were recorded using a smart diamond ATR attachment on a Thermo -Nicolet FT-IR Spectrometer (AVATAR 320) over the range 4000 to 400 cm⁻¹. Mass spectra were performed at EPSRC Mass Spectrometry Service Centre, University of Wales, Swansea and University of Sheffield. The instrument used was the 'WATERS LCT premier', the ionization was electrospray (ESI+), the solvent was water/acetonitrile (1:3), while the ionization was electrospray (ESI+ and ES-) Thermofisher LTQ Orbitrap XL used to analyse volatile molecules in the mass range m/z 50–2000 or m/z 200–4000 Daltons.

2.3 Magnetic susceptibility

Magnetic susceptibility is measured with a Gouy magnetic susceptibility balance. The gram magnetic susceptibility for a substance is calculated from:

$$\chi_{\text{g}} = (\text{C}_{\text{bal}}) (l) (R - R_0) / (10^9) (m)$$

Where l = height of sample in the tube in units of centimeters, m = mass of the sample in units of grams, R = reading for tube plus sample, R_0 = reading for the empty tube and $C_{\text{bal}} =$

balance calibration constant = 1.0. The molar magnetic susceptibility is then calculated from the gram magnetic susceptibility using the following equation.

$$\chi_m = (\chi_g) (\text{molar mass})$$

The effective magnetic moment for a particular substance is calculated from the gram magnetic susceptibility [18] using the following equation (T represents the Kelvin temperature (294 K)):

$$\mu_{\text{eff}} = 2.83 [(\chi_m) (T)]^{1/2}$$

The calculated μ_{eff} values for the L- complexes are given in the experimental characterization data and discussed in section 3.2.

2.4 X-ray diffraction

Single crystal X-ray diffraction measurements for $[\text{MnL}_2\text{Cl}_2]$, $[\text{CoL}_2\text{Cl}_2]$ and $[\text{NiL}_2\text{Cl}_2]$ were performed using a Rigaku Saturn 724+ area detector mounted at the window of an FR-E+ rotating anode generator with a Mo $K\alpha$, $\lambda=0.71075\text{\AA}$. The crystals were mounted on glass fiber and the data were collected at 120K under nitrogen flow from an Oxford Cryosystems cryostream 700 device. An empirical absorption correction was carried out using SADABS and the structures were solved by direct methods using SUPERFLIP [19]. Data were processed and empirical absorption corrections were also done using Crystal Clear SM-Expert, with the unit cell parameters refined against all data [20]. The structures were solved by direct methods using SHELXS-97 with in OLEX2 [21]. All refinements on F_o^2 by full-matrix least squares refinement were solved using the SHELXL-97 program package [22]. All non-hydrogen atoms were refined by isotropic displacement parameters and hydrogen atoms were added at calculated positions. Further refinement was done using a riding model with C-H (aromatic) 0.95\AA $U_{\text{ISO}} = 1.5U_{\text{eq}}(\text{C})$; C-H (methyl) 0.98\AA $U_{\text{ISO}} = 1.5U_{\text{eq}}(\text{C})$. [23]. Perspective drawings of the molecular structures of $[\text{MnL}_2\text{Cl}_2]$, $[\text{CoL}_2\text{Cl}_2]$ and $[\text{NiL}_2\text{Cl}_2]$, also showing the atom numbering scheme used, is shown in Figure 3, Figure 4 and Figure 5. Crystallographic data are presented in Table 3 with selected bond lengths, bond angles and torsion angles in Table 4. Additional crystallographic data is provided in the Electronic Supplementary Information.

2.5 Theoretical approach

Density functional theory (DFT) calculations were performed with the B3LYP functional as implemented in the Gaussian 09 package [24] using the triple- ζ basis set 6-311G(d,p). Since the complexes of this study are paramagnetic, all the different spin states were considered when performing the DFT calculations. The input coordinates for the complexes were constructed using Chemcraft [25].

3 Results and discussion

The 2-(1-(4-methoxy-phenyl)-1H-1,2,3-triazol-1-yl)pyridine-metal complexes of this study were synthesized from a 1:2 mole ratio of the 2-(1-(4-methoxy-phenyl)-1H-1,2,3-triazol-1-yl)pyridine and the metal chloride. Characterization of the product includes FT-IR, MS, NMR, UV-Vis, melting points, magnetic moments, conductivity measurements, solid state X-ray crystal structures and computational chemistry calculations.

3.1 IR Spectral data

The IR spectra of the metal complexes exhibited bands with appropriate shifts due to complex formation (see Table 1 and Supplementary Information Figures S1 – S4). The $\nu(\text{C}=\text{N})_{\text{py}}$ stretching band of the pyridine moiety which is observed at the value around 1604 cm^{-1} in the free ligand, is shifted to higher wavenumbers, around 1612–1607 cm^{-1} for the various complexes. This indicates coordination of the nitrogen of the C=N pyridine moiety to the different metal atoms. The $\nu(\text{C}=\text{C})_{\text{Ar}}$ bands of the phenyl ring for the complexes, which usually appear as two absorptions are around 1598-1580 cm^{-1} and 1500-1470 cm^{-1} , compared with the peak at 1592 cm^{-1} in the free ligand [26,27]. The $\nu(\text{C}=\text{N})_{\text{triaz}}$ absorption band of the triazole moiety around 1574 cm^{-1} in the free ligand is detected around 1572–1576 cm^{-1} in the metal complexes, while the $\nu(\text{C}=\text{C})_{\text{triaz}}$ absorption band of the triazole moieties which appear at 1549 cm^{-1} in the free ligand, is detected around 1551–1557 cm^{-1} in the metal complexes, as indicated in Table 1.

Table 1. IR frequencies in wavenumber (cm^{-1}) units of the ligands (L) and the $[\text{ML}_2\text{Cl}_2]$ complexes.

Compound	$\nu(\text{C}=\text{N})_{py}$, $\nu(\text{C}=\text{C})_{Ar}$, $\nu(\text{C}=\text{N})_{triaz}$ conj.	$\nu(\text{C}=\text{C})_{triaz}$	$\nu(\text{N}-\text{N})_{triaz}$	$\nu(\text{N}=\text{N})_{triaz}$	$\nu(\text{C}-\text{N})$
L^3	1604, 1592, 1574	1549	1154,1022	1515	1258
$[\text{Mn}(L^3)_2\text{Cl}_2]$	1607, 1596, 1576	1555	1157,1030	1518	1254
$[\text{Fe}(L^3)_2\text{Cl}_2]$	1607, 1597, 1572	1556	1147,1028	1518	1261
$[\text{Co}(L^3)_2\text{Cl}_2]$	1609, 1597, 1574	1557	1146,1028	1518	1254
$[\text{Ni}(L^3)_2\text{Cl}_2]$	1612, 1597, 1576	1551	1147,1028	1519	1263

3.2 Magnetic moment

The d^5 $[\text{MnL}_2\text{Cl}_2]$, d^6 $[\text{FeL}_2\text{Cl}_2]$, d^7 $[\text{CoL}_2\text{Cl}_2]$ and d^8 $[\text{NiL}_2\text{Cl}_2]$ are paramagnetic and cannot be characterized by NMR. The magnetic moment values obtained for the complexes are given in **Table 2**. The observed room temperature magnetic moment value of 5.32 B.M for d^5 $[\text{MnL}_2\text{Cl}_2]$ is typical for a high spin configuration of Mn(II)-complexes, and confirm an octahedral geometry about Mn atom [^{28, 29, 30}]. For the d^6 $[\text{FeL}_2\text{Cl}_2]$ complex the magnetic moment of 5.07 B.M indicates a high spin octahedral geometry around the Fe atom [^{31, 32, 33, 34}]. The magnetic measurement of the spin (d^7) Co(II) complex, with the value 3.97 B.M, corresponds to three unpaired electrons. This value is in agreement with a high spin configuration and supports an octahedral environment around the Co(II) ion [^{35, 36}]. The magnetic measurement value 2.73 B.M for d^8 $[\text{NiL}_2\text{Cl}_2]$ corresponds to two unpaired electrons. This value is in agreement with a high spin configuration and confirmed the octahedral environment around the spin (d^8) Ni(II) atom [^{37, 38, 39}].

3.3 UV-Vis Spectral data

UV-visible spectrometry highlights the differences in the ability of the complexes to absorb light. The UV-Vis Spectrum data of the $[\text{ML}_2\text{Cl}_2]$ complexes are presented in **Table 2** and shown in **Figure 2**. The free ligand L, as well as the $[\text{ML}_2\text{Cl}_2]$ complexes have two intra - ligand, $\pi \rightarrow \pi^*$, $n \rightarrow \pi^*$ peaks in the 250 -300 nm range regardless of the metal centre.

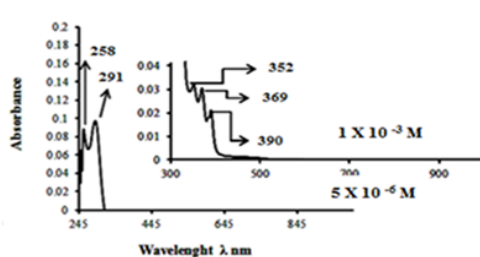
The UV-Vis spectrum of the Mn(II) complex in **Figure 2** (a) exhibits two bands at 258 nm, and 291 nm at concentration of 5×10^{-6} M. These bands are related to the intra ligand transitions $\pi \rightarrow \pi^*$ and $n \rightarrow \pi^*$, respectively. High spin Mn(II)-complexes are very weakly

coloured compounds due to spin forbidden d-d transitions. Therefore, it is difficult to identify the d-d bands of the Mn(II) complex. At higher concentrations of the Mn(II)-complex, e.g at a concentration of 1×10^{-3} M, the complex displays several bands. The first band at 352 nm = 28409 cm^{-1} ; $\epsilon_{\text{max}} = 32 \text{ dm}^3 \text{ mol}^{-1} \text{ cm}^{-1}$, is assignable to an $n \rightarrow \pi^*$ transition. The metal-ligand charge transfer transition band is observed at 369 nm = 27100 cm^{-1} ; $\epsilon_{\text{max}} = 30 \text{ dm}^3 \text{ mol}^{-1} \text{ cm}^{-1}$. Lastly the band detected at 390 nm = 25641 cm^{-1} ; $\epsilon_{\text{max}} = 21 \text{ dm}^3 \text{ mol}^{-1} \text{ cm}^{-1}$ could be attributed to a ${}^4A_{1g} \rightarrow {}^4T_{1g}$ transfer.

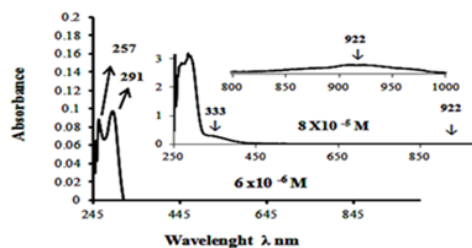
The UV-Vis spectrum of the Fe(II) complex gave a yellow colour in DMSO solution, and is shown in **Figure 2** (b). The spectrum reveals two absorption peaks at 257 and 291 nm, which are assigned to the intraligand $\pi \rightarrow \pi^*$ and $n \rightarrow \pi^*$ transitions (red shift). The absorption peak at 333 nm is related to the charge transfer transition. The peak detected at 922 nm is attributable to a ${}^5T_{2g} \rightarrow {}^5E_{2g}$ transfer.

The spectra of the Co(II) complex depicted in **Figure 2** (c), show intraligand transitions. The Co-complex displays two additional bands in the visible region at 615 and 678 nm, which are related to ${}^4T_{1g}^{(F)} \rightarrow {}^4T_{2g}^{(P)}$ and ${}^4T_{1g}^{(F)} \rightarrow {}^4A_{2g}^{(F)}$ transitions respectively. This is characteristic for the distorted octahedral geometry around the Co atom.

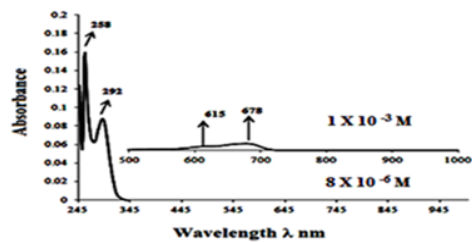
In addition to the intraligand transitions, the Ni(II) complex, **Figure 2** (d), has a further two absorbance peaks, the first being at 407 nm and the second at 660 nm, attributed to ${}^3A_{2g}^{(F)} \rightarrow {}^3T_{1g}^{(P)}$ and ${}^3A_{2g}^{(F)} \rightarrow {}^3T_{1g}^{(F)}$ transitions, respectively. This is typical for a distorted octahedral geometry around the Ni atom [40]



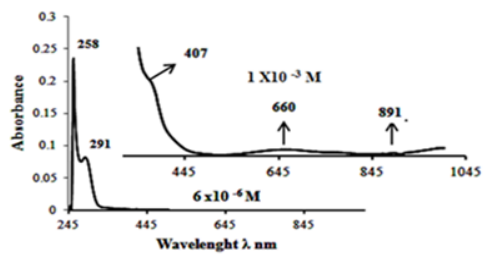
(a) $[\text{MnL}_2\text{Cl}_2]$



(b) $[\text{FeL}_2\text{Cl}_2]$



(c) $[\text{CoL}_2\text{Cl}_2]$



(d) $[\text{NiL}_2\text{Cl}_2]$

Figure 2: UV-Vis spectra of the $[\text{ML}_2\text{Cl}_2]$ complex in DMSO solutions.

Table 2. UV-Vis spectral data of L complexes in DMSO solutions.

Compound	Band Position λ_{\max} (nm)	Wave number (cm ⁻¹)	Extinction coefficient ϵ_{\max} (dm ³ mol ⁻¹ cm ⁻¹)	Assignment	μ_{eff} B.M.
L	285	35087	24375, (4x10 ⁻⁶ M)	Intra - ligand, $\pi \rightarrow \pi^*$, n $\rightarrow \pi^*$	
[MnL ₂ Cl ₂]	258, 291	38759, 34364	6210, 3059, (5x10 ⁻⁶ M)	Intra - ligand, $\pi \rightarrow \pi^*$, n $\rightarrow \pi^*$	5.32
	352,	28409,	32, 1x10 ⁻³ M)	CT	
	369	27100	30, (1x10 ⁻³ M)	${}^6A_{1g} \rightarrow {}^4T_{1g}$	
	390	25641	21, (1x10 ⁻³ M)		
[FeL ₂ Cl ₂]	257, 291	39062, 34364	35500, 17500, (6x10 ⁻⁶ M)	Intra - ligand, $\pi \rightarrow \pi$, n $\rightarrow \pi^*$	5.07
	333	30030	3810, (8x10 ⁻⁵ M)	CT	
	922	10845	65, (8x10 ⁻⁵ M)	${}^5T_{2g} \rightarrow {}^5E_{2g}$	
[CoL ₂ Cl ₂]	257, 292	38910, 34246	26625, 11000, (8x10 ⁻⁶ M)	Intra - ligand $\pi \rightarrow \pi^*$, n $\rightarrow \pi^*$	3.97
	615	16260	38, (1x10 ⁻³ M)	${}^4T_{1g}^{(F)} \rightarrow {}^4T_{1g}^{(P)}$	
	677	14771	61, (1x10 ⁻³ M)	${}^4T_{1g}^{(F)} \rightarrow {}^4A_{2g}^{(F)}$	
[NiL ₂ Cl ₂]	257, 291	39682, 34364	30000, 18167 (6x10 ⁻⁶ M)	Intra-ligand $\pi \rightarrow \pi^*$, n $\rightarrow \pi^*$	2.73
	407	24570	61, (1x10 ⁻³ M)	$A_{2g}^{(F)} \rightarrow {}^3T_{1g}^{(P)}$	
	660	15151	43, (1x10 ⁻³ M)	${}^3A_{2g}^{(F)} \rightarrow {}^3T_{1g}^{(F)}$	

3.4 X-ray structures

The molecular structure of the complexes [MnL₂Cl₂], [CoL₂Cl₂] and [NiL₂Cl₂] can be described as distorted octahedral. The structures of [CoL₂Cl₂] and [NiL₂Cl₂] have the two bidentate triazole ligands in the equatorial plane and the two chloro ligands in the axial positions *trans* to each other. However, in [MnL₂Cl₂], the two chloro ligands are adopting the *cis* positions around the Mn centre. Perspective drawings of the molecular structures, also showing the atom numbering scheme, are given in Figure 3 (*cis* [MnL₂Cl₂]), Figure 4 (*trans* [CoL₂Cl₂]) and Figure 5 (*trans* [NiL₂Cl₂]). Crystallographic data are presented in Table 3 with selected bond lengths, bond angles and torsion angles in Table 4. Data of the related complex *trans* [FeL₂Cl₂] and L is added in Table 4 for comparative purposes. Additional crystallographic data is provided in the Electronic Supplementary Information. The *trans* [CoL₂Cl₂] and *trans* [NiL₂Cl₂] structures presented here will be compared to the related *trans* [FeL₂Cl₂] structure [11]. It is the first time that a *cis* orientation of the (1,2,3-triazol-4-yl)pyridine ligands and the halogen atoms has been found for an octahedral Mn(II), Fe(II), Co(II) or Ni(II) complex containing two bidentate (1,2,3-triazol-4-yl)pyridine ligands and two halogen atoms. The only other known crystal structure of an octahedral Mn(II), Fe(II), Co(II) or Ni(II) complex containing two bidentate (1,2,3-triazol-4-yl)pyridine ligands and two halogen atoms [41], is that of a Ni(II) complex, dibromo(bis{2-[1-(4-cyclohexyl)-1H-1,2,3-triazol-4-yl-kN3]pyridine-kN})nickel(II), that also has a *trans* orientation of the halogen (bromo) atoms with the triazole ligands in the equatorial plane [42].

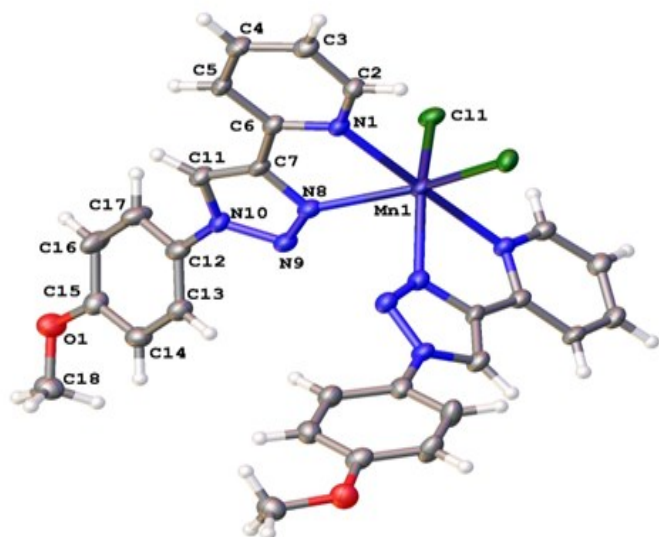


Figure 3. A labelled molecular structure diagram of $[\text{MnL}_2\text{Cl}_2]$ with displacement thermal ellipsoids drawn at 50% probability.

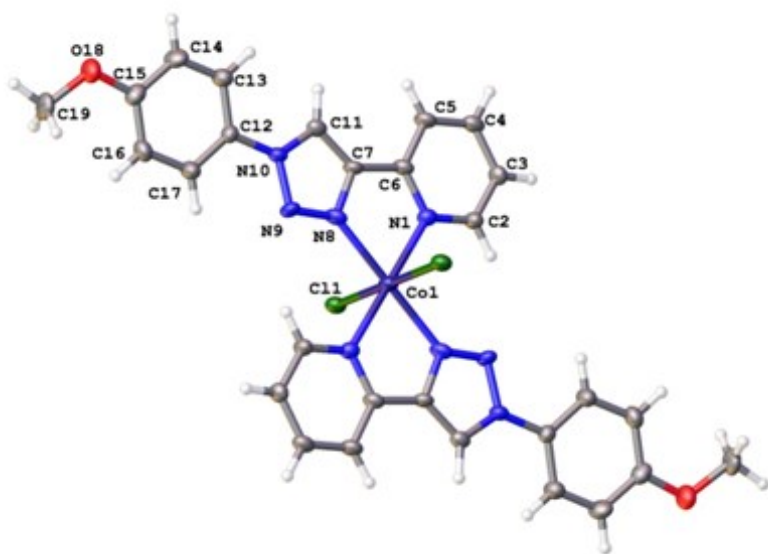


Figure 4. A labelled molecular structure diagram of $[\text{CoL}_2\text{Cl}_2]$ with displacement thermal ellipsoids drawn at 50% probability. The asymmetric unit consists of one half of the complex with the other half generated by symmetry and the Ni atom lying on an inversion centre.

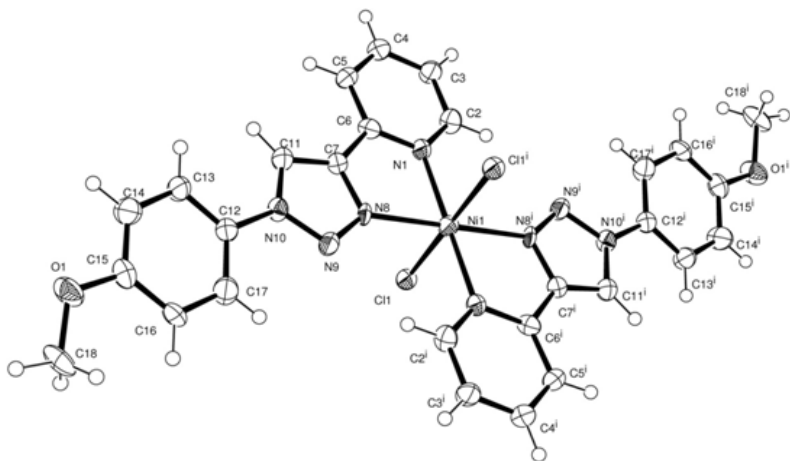


Figure 5. The molecular structure of $[\text{NiL}_2\text{Cl}_2]$. The thermal ellipsoids are drawn at a 50% probability. The asymmetric unit consists of one half of the complex with the other half generated by symmetry and the Ni atom lying on an inversion centre.

Table 3. Crystallographic data for the complexes.

Compound	$[\text{MnL}_2\text{Cl}_2]$	$[\text{CoL}_2\text{Cl}_2]$	$[\text{NiL}_2\text{Cl}_2]$
Empirical formula	$\text{C}_{28}\text{H}_{24}\text{Cl}_2\text{MnN}_8\text{O}_2$	$\text{C}_{28}\text{H}_{24}\text{Cl}_2\text{CoN}_8\text{O}_2$	$\text{C}_{28}\text{H}_{24}\text{Cl}_2\text{NiN}_8\text{O}_2$
M_r	630.39	634.38	634.16
Temp/K	100 K	100(2) K	100(2) K
Cryst. syst.	Orthorhombic	Monoclinic	Monoclinic
Space group	$Pbcn$	$P2_1/c$	$P2_1/c$
$a/\text{\AA}$	13.4618(9)	10.3480(10)	10.459(15)
$b/\text{\AA}$	9.2130(6)	12.9032(12)	12.968(17)
$c/\text{\AA}$	22.9298(16)	10.1969(9)	10.350(15)
$\alpha/^\circ$	90.00	90.00	90.00
$\beta/^\circ$	90.00	95.772(7) $^\circ$	95.61(3)
$\gamma/^\circ$	90.00	90.00	90.00
$V/\text{\AA}^3$	2843.8(3)	1354.6(2)	1397(3)
Z	4	2	2
R_{int}	0.1012	0.2085	0.1445
$D_{\text{calcd}}/\text{g cm}^{-3}$	1.472	1.555	1.508
Refln (all/ind)	12965/ 3242	15422/ 3098	7036/ 3134
μ/mm^{-1}	1.000-0.092	0.875	0.928
$R1/wR2$	0.0597/ (obsd data: $F^2 >$	0.0466/ 0.0762	0.0928/ 0.1629
$2\sigma(F^2)^a$	0.1345		
$R1/wR2$ (all data) ^a	0.1127/ 0.1624	0.1516/ 0.0886	0.1772/ 0.2084

Table 4. Selected bond lengths (\AA), bond and torsion angles ($^\circ$) for the $[\text{ML}_2\text{Cl}_2]$ complexes and the L ligand.

	L	[MnL ₂ Cl ₂]	[FeL ₂ Cl ₂] ^a	[CoL ₂ Cl ₂]	[NiL ₂ Cl ₂]
Bond distance (Å)					
C7–C11	1.362(6)	1.371(5)	1.375(3)	1.360(4)	1.361(9)
N8–N9	1.302(4)	1.305(4)	1.311(2)	1.309(4)	1.331(7)
N9–N10	1.355(4)	1.358(4)	1.354(2)	1.362(3)	1.368(7)
N8–C7	1.365(5)	1.365(4)	1.360(2)	1.360(3)	1.370(8)
M–N _(PY) 1		2.330(3)	2.2018(15)	2.127(2)	2.1015(19)
M–N _(triazole) 1		2.324(3)	2.1838(16)	2.105(3)	2.0739(19)
M–Cl1		2.4544(11)	2.4456(5)	2.4398(10)	2.4123(6)
Bond angle (°)					
N _(PY) 1 –M–N _(PY) 1 ⁱ		178.89(16)	180.0	179.999(1)	179.999(1)
N _(triazole) 1 ⁱ –M–N _(triazole) 1		87.13(15)	180.0	179.999(1)	179.999(1)
N _(PY) 1–M–N _(triazole) 1 ⁱ		108.95(11)	104.10(6)	102.93(10)	101.3(2)
N _(PY) 1 –M–N _(triazole) 1		71.90(10)	75.90(6)	77.07(10)	78.7(2)
N _(PY) 1–M– Cl 1		91.05(8)	89.80(4)	90.32(8)	90.28(15)
N _(PY) 1 ⁱ –M– Cl 1		88.30(8)	90.20(4)	89.68(8)	89.72(15)
N _(triazole) 1 ⁱ –M– Cl 1		155.71(8)	90.20(4)	90.25(9)	89.36(18)
N _(triazole) 1 –M– Cl 1		86.19(8)	89.80(4)	89.75(9)	90.64(18)
Cl 1 ⁱ –M– Cl 1		108.66(6)	180.0	179.999(1)	180.0
N _(PY) 1 –M–Cl ₂					
N _(triazole) 8 –M–Cl ₂					
Torsion angle (°)					
N(t) 1i–M–N(p) 1– C2		96.3(3)	0.6(3)	0.23(17)	1.7(6)
N(t) 1 –M–N(p) 1– C2		176.6(3)	–179.4(3)	–179.77(17)	–178.3(6)
Cl 1i–M–N(p) 1– C2		10.9(3)	–89.1(3)	90.07(15)	92.3(5)
Cl 1–M–N(p) 1– C2		–97.8(3)	90.9(3)	–89.93(15)	–87.7(5)
N(t) 1i–M–N(t) 1–N9		–75.5(3)	101(16)	–74(7)	21(6)
N(p) 1 –M–N(t) 1–N9		173.5(4)	–179.6(4)	179.5(2)	179.7(6)
N(p) 1i–M–N(t) 1–N9		–5.8(4)	0.4(4)	–0.5(2)	–0.3
Cl 1i–M–N(t) 1–N9		–149.7(3)	90.8(4)	–90.40(18)	–90.4(6)
Cl 1 –M–N(t) 1–N9		81.1(3)	–89.2(4)	89.60(18)	89.6(6)
M–N(t) 1–N9–N10		–160.6(3)	177.0(3)	179.13(13)	176.7(4)
N8–N9–N10– Cl1		–0.4(4)	–0.4(4)	–0.1(2)	–179.7(5)
N8–N9–N10– Cl2		–179.8(3)	179.1(3)	179.67(16)	0.7(10)

a Data from reference [11].

3.4.1 *Cis* [MnL₂Cl₂]

Cis [MnL₂Cl₂] crystallised in an orthorhombic space group *Pbcn* with four molecules per unit cell. The geometry about the Mn atom is essentially a distorted octahedral coordination arrangement with a twofold symmetry axis, *C*₂, through Mn. The octahedral basal plane is formed by the two Cl atoms Cl1 and Cl1ⁱ, which are arranged in the *cis* position to each other and two nitrogen atoms N8 and N8ⁱ. The remaining two vacant sites on the metal centre are occupied by the nitrogen atoms N1 and N1ⁱ of the pyridyl moieties adopting a *trans* position with a 178.89(16)° angle between N1^{ax}–Mn1–N1ⁱ^{ax}. The ligand-metal-ligand angles in *cis* [MnL₂Cl₂] deviate significantly from the ideal value of 90° or 180° (characteristic of a regular octahedron), see Table 4. Consequently, the 2-(1-(4-methoxy-phenyl)-1H-1,2,3-triazol-1-yl)pyridine ligands fold around the metal ion in a *cis* conformation, allowing the N triazoles to form an equatorial plane with the Cl[–] anions. Completing the remaining axial sites on the manganese atom are the N atoms of the pyridyl moieties.

The bite angle N8–Mn–N1 within the coordinated 2-(1-(4-methoxy-phenyl)-1H-1,2,3-triazol-1-yl)pyridine ligands is 71.90(10)°. Consequently the Cl1–Mn1–Cl1 angle of 108.66(6)° is slightly higher than the angles found for octahedral Mn(II) complex having *cis* chloride atoms (for example CSD reference codes CIQWUW, MAMNCH, PYMNCH10, QUMNCL, TMAMNC, YAJTUA with angles between 89 and 96°⁴³) [44]. The bond length of the terminal chloro groups, Mn–Cl1 and Mn–Cl1i, is 2.4544(11) Å. The bond lengths of N8–N9, N9–N10 and N8–C7 of the 1,2,3-triazole segment are 1.305(4) Å, 1.358(4) Å and 1.365(5) Å, respectively. These distance values are similar to the distances for the free ligand, namely 1.302(4) Å, 1.355(4) Å and 1.365(5) Å respectively. The Mn–N_{py} and Mn–N_{triazole} bond lengths of 2.330(3) Å and 2.324(3) Å are fairly standard [45][46][47]. The metal-triazole bond length is slightly shorter than the metal pyridine bond (by approximately 0.006 Å). The angles between the pyridine plane and the triazole ring and between the triazole plane and the substituted phenyl ring are 115.4(3)° and 120.5(3)°, respectively. The dihedral angle between the plane of the pyridyl moiety and the mean plane of the triazole ring is 5.4(5)°. Furthermore, the dihedral angle between the plane of methoxy phenyl group and the plane of the triazole moiety is tilted by 38.6(5)°.

In the crystal the molecules are arranged in infinite hydrogen-bonded 3D supramolecular chains along the b-axis direction, and within the chains are weak intermolecular $\pi \dots \pi$ interactions and C–H...Cl hydrogen bonding interactions, see Figure 6. The packing resulted in an offset-slipped parallel alignment of the phenyl rings, stabilised by phenyl-phenyl $\pi \dots \pi$ interactions between the (C₁₂C₁₃C₁₄C₁₅C₁₆C₁₇) and the (C₁₂C₁₃C₁₄C₁₅C₁₆C₁₇) phenyl rings with a centroid – centroid distance of 3.985 Å. On the other hand, the chelated (triazole) segment, which does not take part in the $\pi \dots \pi$ interactions, is involved in a (D–H...A) interaction. There are no classic hydrogen bonds, but there are intermolecular interactions of the type D–H...A, which include C–H...Cl, C–H...O and C–H...N hydrogen bonds, see Table 5 and Figure 6. The identified hydrogen bonds are C3–H3...O1, C18–H18A...Cl1, C11–H11...Cl1, C4–H4...N9 and C5–H5A...Cl1 with angles prefer values ranging from 90° to 130° [48,⁴⁸ 49].

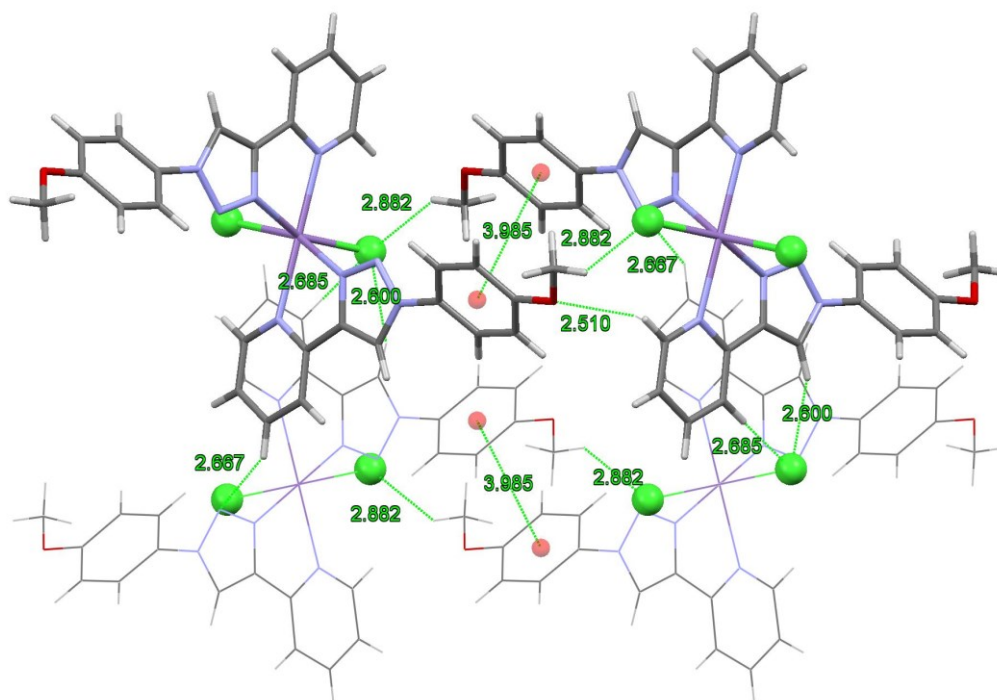


Figure 6. Partial packing in $[\text{MnL}_2\text{Cl}_2]$ showing selected intermolecular hydrogen bonding and $(\pi \dots \pi)$ stacking interactions. The given distances are in Å. The complex is viewed along the crystallographic b -axis. Color code: $(\text{C}_{12}\text{C}_{13}\text{C}_{14}\text{C}_{15}\text{C}_{16}\text{C}_{17})$ centroids (red dots), Cl (green balls), C (grey), N (blue), O (red) and H (white).

Table 5. Hydrogen bonding interactions parameters; D= donor and A= acceptor (Å, °) in the complex $[\text{MnL}_2\text{Cl}_2]$.

D-H...A	D-H	H-A	D-A	Angle
C3-H3...O1	0.950(4)	2.510(3)	3.540 (8)	159.0(2)
C18-H18A...Cl1	0.981(4)	2.882(9)	3.700(4)	141.4(2)
C5-H5...Cl1	0.950(3)	2.685(1)	3.620 (4)	168.3(2)
C4-H4... N9	0.949(4)	2.947(3)	3.787(8)	128.3(2)
C11-H11... Cl1	0.950(4)	2.599(8)	3.490(1)	156.2(4)
Mn-Cl...H5				96.75(4)
Mn-Cl...H11				115.89(4)
Mn-Cl...H18A				91.59(3)

3.4.2 *Trans* $[\text{CoL}_2\text{Cl}_2]$ and *trans* $[\text{NiL}_2\text{Cl}_2]$

The X-ray molecular structure of *trans* $[\text{CoL}_2\text{Cl}_2]$ (Figure 4) and *trans* $[\text{NiL}_2\text{Cl}_2]$ (Figure 5) are merely identical as can be seen from molecular structure overlay of the two molecules in Figure 7 (top). Both molecules crystallise in the monoclinic $P2_1/c$ space group with a distorted octahedral coordination arrangement round the metal, and two molecules per unit cell. Due to inversion symmetry through the metal center, the asymmetric unit consists of one half of the complex with

the other half generated by inversion symmetry. The six atoms coordinated to the metal center is C11 and C11ⁱ, N8_{triazole} and N8_{triazole}ⁱ, N1_{PY} and N1_{PY}ⁱ. Nitrogens N8_{triazole} and N1_{PY} belong to the triazole and pyridyl groups of the bidentate 2-(1-(4-methoxy-phenyl)-1H-1,2,3-triazol-4-yl)pyridine ligand L. In the equatorial plane, the pyridine N1_{PY} and N8_{TA} donors from the two ligands are mutually *trans* to each other, similar as observed for *trans* [FeL₂Cl₂] [11]. The angles between the different nitrogens in the equatorial plane, namely N8_{triazole}^{eq}–Ni–N1_{PY}^q and N8_{triazole}^{i,eq}–Ni–N1_{PY}^{eq} are 77.07(10)° and 102.93(10)° for Co and 78.7(2)° and 101.3(2)° for Ni respectively. These angles between the different nitrogens in the equatorial plane, deviates from the 90° angle for a real octahedron, because of the chelating nature of the two L ligands. The axial positions are occupied by two chloride ions C11–Ni–C11ⁱ, and due to inversion symmetry, the angle is 180.0° for both structures. The X-ray molecular structure of *trans* [FeL₂Cl₂], *trans* [CoL₂Cl₂] and *trans* [NiL₂Cl₂] are very similar (compare the data in Table 4), with a slight difference in the orientation of the 4-methoxy-phenyl groups, see Figure 7 (middle). The dihedral angle between the mean plane of the pyridyl moiety and the mean plane of the triazole ring in the coordinated 2-(1-(4-methoxy-phenyl)-1H-1,2,3-triazol-1-yl)pyridine ligand is 0.66° for [FeL₂Cl₂], 0.35° for [CoL₂Cl₂] and 1.69° for [NiL₂Cl₂], leading to conjugation throughout the triazole–pyridyl backbone. The angle between the near planar pyridine-triazole plane and the 4-methoxyphenyl ring is 11.79° for [FeL₂Cl₂], 13.13° for [CoL₂Cl₂] and 15.65° for [NiL₂Cl₂]. The X-ray molecular structure of *trans* [FeL₂Cl₂], *trans* [CoL₂Cl₂] and *trans* [NiL₂Cl₂] are very similar to that of the related *trans* dibromo(bis{2-[1-(4-cyclohexyl)-1H-1,2,3-triazol-4-yl-kN3]pyridine-kN})nickel(II) structure [42], containing cyclohexyl instead of the *para*-ethoxy-group-attached at the N10 nitrogen of the triazole group, see Figure 7 (bottom).

The bond lengths of N8–N9, N9–N10 and N8–C7 of the 1,2,3-triazole ring in the free ligand are very similar to the related bonds in the [ML₂Cl₂] complexes, only in [NiL₂Cl₂] these values are slightly higher (by approximately 0.028 Å), see values in Table 4. In the *trans* [ML₂Cl₂] complexes (M = Fe, Co or Ni), the Ni–Cl bond lengths varies from 2.41 – 2.45 Å, the Ni–N_{PY} bond lengths from 2.10-2.20 Å, while the Ni–N_{triazole} bond lengths are between 2.07 and 2.18 Å. In a specific complex the metal-triazole bond length is slightly shorter than the metal-pyridine bond length (by approximately 0.02 Å).

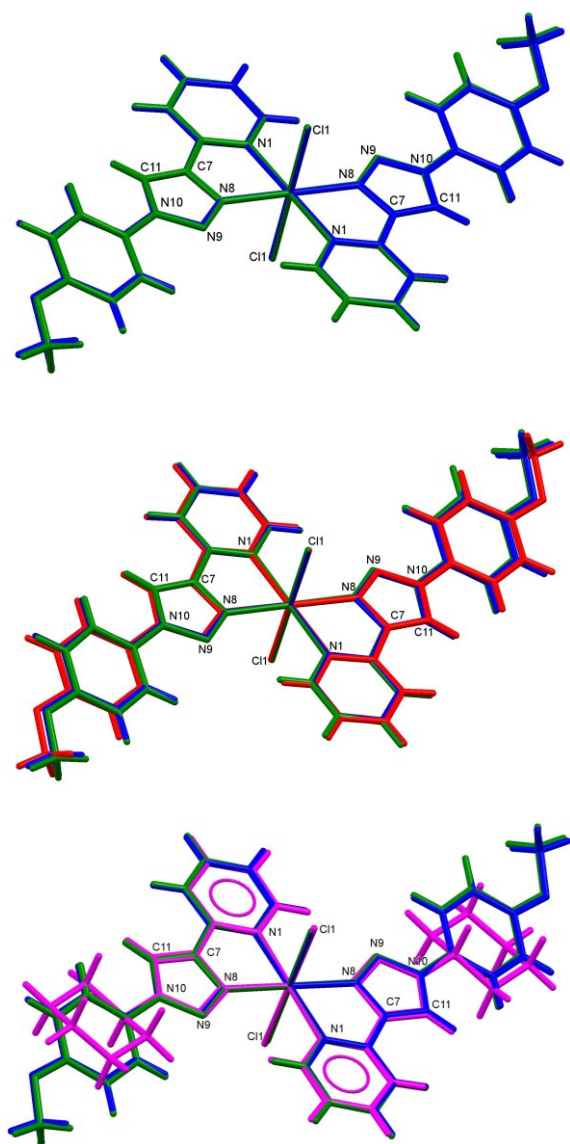


Figure 7. Top. Overlay of the structures of *trans* [CoL₂Cl₂] (blue) and *trans* [NiL₂Cl₂] (green). The root means square (RMS) overlay values, when using the six atoms of the octahedral coordination polyhedron, is 0.038. Middle. Overlay *trans* [CoL₂Cl₂] (blue), *trans* [NiL₂Cl₂] (green), and *trans* [FeL₂Cl₂] (red) [11]. Bottom. Overlay *trans* [CoL₂Cl₂] (blue), *trans* [NiL₂Cl₂] (green), and *trans* dibromo(bis{2-[1-(4-cyclohexyl)-1H-1,2,3-triazol-4-yl-kN3]pyridine-kN})nickel(II) (magenta) [42].

An extensive network of weak hydrogen bonding interactions ^{[50][51]} generates a 3D supramolecular sheet in the solid state for both [CoL₂Cl₂] and [NiL₂Cl₂]. The hydrogen bonding can be described as follows for [CoL₂Cl₂] (similar for [NiL₂Cl₂] and [FeL₂Cl₂]):

(a) Each chloride atom of one molecule is hydrogen-bonded to three molecules in the next layer, namely (i) to the C4–H4 group of the pyridyl ring (2.935 Å) of one molecule, (ii) C19–H19 of the methoxy group (2.916 Å) of another molecule and (iii) to the C11–H11 on a triazole ring (2.549 Å),

(iv) C5-H5 of the pyridyl ring (3.560 Å) and (v) C13-H13 of the phenyl ring (2.852 Å) of a third molecule, see Figure 8. Most of these bonds are below the sum of the Van der Waals radii of H and Cl of 3 Å [52].

(b) The different layers of molecules are held together by hydrogen bonds between C18-H18 of the methoxy group and N9 of the a triazole ring (2.589 Å), see Figure 9. The latter N-H interaction is also below sum of the Van der Waals radii of H and N of 2.75 Å.

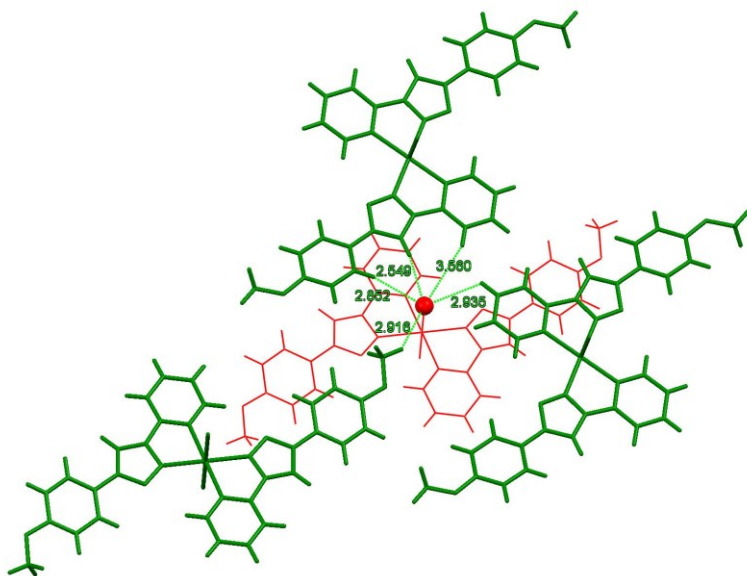


Figure 8. Partial packing diagram of [CoL₂Cl₂] showing intermolecular hydrogen bonding interactions to chloride of a molecule (red) in the bottom layer to three different molecules (green) in the top layer.

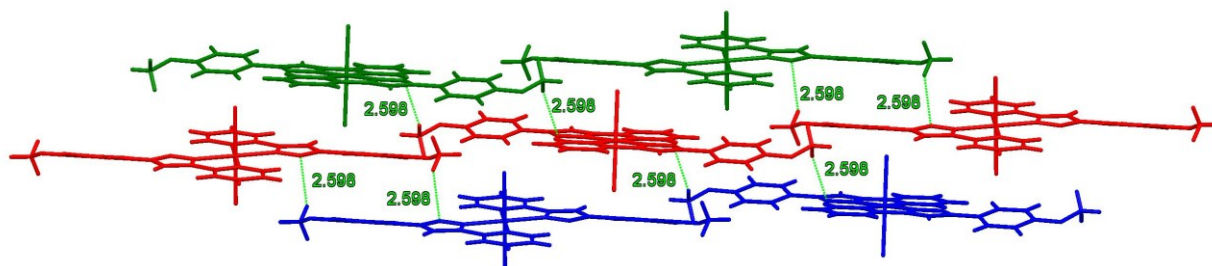


Figure 9. A 3D supramolecular sheet in [CoL₂Cl₂] complex showing intermolecular hydrogen bonding interactions between layers.

The overlap between the triazole N₈N₉N₁₀C₇C₁₁ and pyridine N₁C₂C₃C₄C₅C₆ rings of the neighbouring molecules resulted in face-to-face and slipped-type parallel alignment. The

interaction between the layers are further strengthened by triazole – pyridine and triazole – phenyl $\pi \dots \pi$ stacking of 3.545 Å and 4.149 Å respectively for $[\text{CoL}_2\text{Cl}_2]$ (Figure 10) and 3.589 Å and 4.258 Å respectively for $[\text{NiL}_2\text{Cl}_2]$. This distance is comparable to the previously reported bond separations of a typical $\pi \dots \pi$ stacking [53][54][55][56].

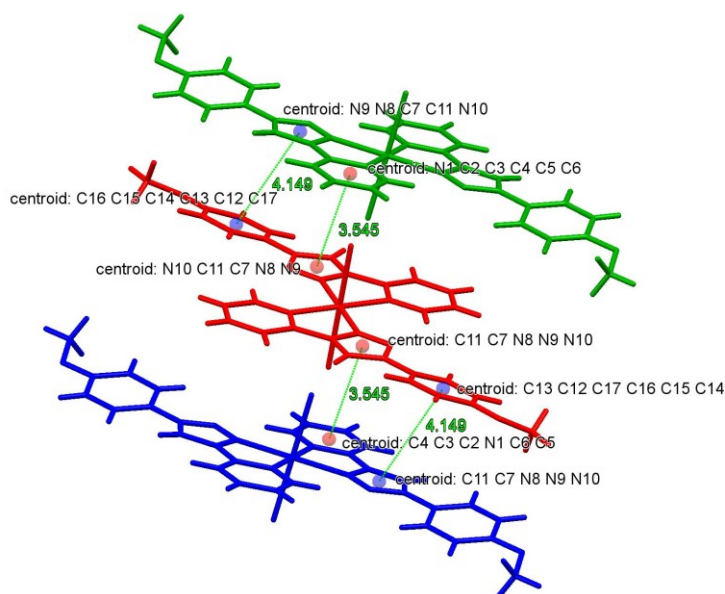


Figure 10. Partial packing diagram of $[\text{CoL}_2\text{Cl}_2]$ showing $\pi \dots \pi$ stacking (distance in Å) involving the triazole - pyridyl and phenyl - triazole rings.

3.5 DFT study

Five geometrical isomers, three *cis* and two *trans*, are possible for the Fe complexes of this study, containing two bidentate (1,2,3-triazol-4-yl)pyridine ligands and two chloride atoms. The isomers are defined by the relative positions of (i) the chloro atoms, (ii) the pyridyl nitrogen and (iii) the triazole nitrogen around the metal, see Figure 11. Experimental magnetic moment measurements showed that the four $[\text{ML}_2\text{Cl}_2]$ complexes of this study are all paramagnetic. To support the experimental assignment of the spin state of the complexes, computational chemistry calculations using density functional theory (DFT) calculations have been done for all the possible spin states of each isomer of the dichloro{bis[2-(1-phenyl-1H-1,2,3-triazol-4-yl-kN3)pyridine-kN]}metal(II), $[\text{M}(\text{L}^1)_2\text{Cl}_2]$, without a methoxy substituent on the phenyl ring ($\text{L}^1 = 2\text{-(1-phenyl-1H-[1,2,3-triazol]-4-yl)pyridine}$). The DFT results, summarized in Table 6, support experimental measurements, showing that

- (i) d^5 $[\text{Mn}(\text{L}^1)_2\text{Cl}_2]$ is high spin with $S = 5/2$, i.e. five unpaired electrons,
- (ii) d^6 $[\text{Fe}(\text{L}^1)_2\text{Cl}_2]$ is high spin with $S = 2$, i.e. four unpaired electrons,

(iii) d^7 $[\text{Co}(\text{L}^1)_2\text{Cl}_2]$ has a spin state of $S = 3/2$, i.e. three unpaired electrons,

(iv) d^8 $[\text{Ni}(\text{L}^1)_2\text{Cl}_2]$ has a spin state of $S = 1$, i.e. two unpaired electrons and

(v) for all $[\text{M}(\text{L}^1)_2\text{Cl}_2]$ complexes, the either *cis-cis-trans* or the *trans-trans-trans* isomers have the lowest energy. In both these isomers the pyridyl groups are *trans* to each other.

For $[\text{Mn}(\text{L}^1)_2\text{Cl}_2]$, the *cis-cis-trans* isomer is preferred by about 0.1 eV, in agreement with the *cis* $[\text{MnL}_2\text{Cl}_2]$ structure obtained in this study. The *trans-trans-trans* isomer is preferred by a very small amount of energy (less than 0.1 eV) for $[\text{Fe}(\text{L}^1)_2\text{Cl}_2]$, $[\text{Co}(\text{L}^1)_2\text{Cl}_2]$ and $[\text{Ni}(\text{L}^1)_2\text{Cl}_2]$.

Additional DFT calculations for the lowest energy spin state of each isomer of the dichloro {bis[2-(1-(4-methoxyphenyl)-1H-1,2,3-triazol-4-yl-kN3)pyridine-kN]} metal(II), $[\text{M}(\text{L})_2\text{Cl}_2]$, with a methoxy substituent on the phenyl ring ($\text{L} = 2$ -(1-(4-methoxyphenyl)-1H-[1,2,3-triazol]-4-yl)pyridine), Table 7, are in agreement with conclusion (v) above. The lowest energy isomer for $\text{Mn}(\text{L})_2\text{Cl}_2$, $[\text{Co}(\text{L}^1)_2\text{Cl}_2]$ and $[\text{Ni}(\text{L}^1)_2\text{Cl}_2]$ is the *cis-cis-trans*, *trans-trans-trans* and *trans-trans-trans* isomer respectively, in agreement with the experimental structures presented in this study.

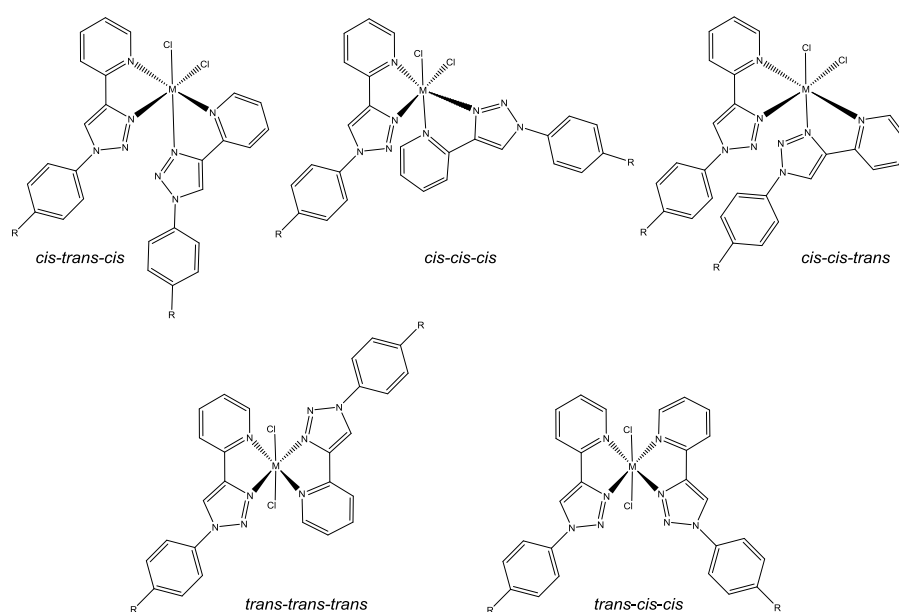


Figure 11. The five geometrical isomers possible for $[\text{ML}_2\text{Cl}_2]$ complexes. $\text{R} = \text{H}$ for $\text{L}^1 = 2$ -(1-phenyl-1H-[1,2,3-triazol]-4-yl)pyridine) and $\text{R} = \text{OCH}_3$ for $\text{L} = 2$ -(1-(4-methoxy-phenyl)-1H-1,2,3-triazol-1-yl)pyridine.

Table 6. Relative Electronic energy E and Gibbs energy G for the indicated spin states and geometrical isomers of $[\text{M}(\text{L}^1)_2\text{Cl}_2]$. $\text{L}^1 = 2$ -(1-phenyl-1H-[1,2,3-triazol]-4-yl)pyridine. The energy of the lowest energy isomer is indicated in bold font.

Isomer ^a	S	E (eV)	G (eV)	E (eV)	G (eV)	S	E (eV)	G (eV)	E (eV)	G (eV)
---------------------	---	--------	--------	--------	--------	---	--------	--------	--------	--------

		Mn		Co			Fe ^b		Ni	
<i>ctc</i>	1/2	1.90	2.11	1.07	1.12	0	1.11	1.35	1.20	1.20
<i>ccc</i>		1.69	1.92	0.80	0.88		0.88	1.12	1.21	1.25
<i>cct</i>		1.49	1.72	0.71	0.79		0.63	0.88	0.97	1.03
<i>ttt</i>		1.35	1.57	0.56	0.64		0.61	0.83	0.93	0.95
<i>tcc</i>		1.64	1.87	0.74	0.79		0.89	1.12	1.11	1.09
<i>ctc</i>	3/2	1.78	1.80	0.45	0.43	1	1.18	1.26	0.50	0.50
<i>ccc</i>	d	d	d	0.24	0.24		0.97	1.07	0.29	0.29
<i>cct</i>	d	d	d	0.04	0.05		0.78	0.88	0.06	0.07
<i>ttt</i>		2.19	2.34	0.00	0.00		1.95	2.09	0.00	0.00
<i>tcc</i>		1.64	1.74	0.22	0.20		0.91	0.98	0.25	0.25
<i>ctc</i>	5/2	0.33	0.31	-	-	2	0.48	0.44	-	-
<i>ccc</i>		0.17	0.15	-	-		0.27	0.26	-	-
<i>cct</i>		0.00	0.00	-	-		0.10	0.10	-	-
<i>ttt</i>		0.14	0.07	-	-		0.00	0.00	-	-
<i>tcc</i>	c	c	c	-	-		0.19	0.16	-	-

a See Figure 11 for the geometry of the different isomers, R = H.

b from reference [11].

c optimized to the *cct* isomer

d geometry did not converge

Table 7. Relative Electronic energy E and Gibbs energy G for the indicated spin states and geometrical isomers of [M(L)₂Cl₂]. L = 2-(1-(4-methoxy-phenyl)-1H-1,2,3-triazol-1-yl)pyridine. The energy of the lowest energy isomer is indicated in bolt font.

Isomer ^a	E (eV)	G (eV)	E (eV)	G (eV)	E (eV)	G (eV)	E (eV)	G (eV)
	Mn S = 5/2		Co S = 3/2		Fe S = 4/2		Ni S = 1	
<i>ctc</i>	0.33	0.30	0.43	0.40	0.57	0.54	0.49	0.46
<i>ccc</i>	0.16	0.15	0.24	0.22	0.38	0.37	0.29	0.28
<i>cct</i>	0.00	0.00	0.04	0.02	0.00	0.00	0.06	0.05
<i>ttt</i>	0.14	0.10	0.00	0.00	0.11	0.12	0.00	0.00
<i>tcc</i>	b	b	0.24	0.21	0.32	0.26	0.27	0.25

a See Figure 11 for the geometry of the different isomers, R = CH₃.

b optimized to the lowest energy *cct* isomer

4 Summary

Three new first row high spin, octahedral metal(II) complexes containing the 2-(1-(4-methoxy-phenyl)-1H-1,2,3-triazol-1-yl)pyridine chromophore as bidentate ligand (L), have been successfully synthesized and characterized. The molecular structures of [CoL₂Cl₂] and [NiL₂Cl₂] have the two bidentate triazole ligands in the equatorial plane and the two chloro ligands in the axial positions *trans* to each other (*trans-trans-trans* isomers), while in [MnL₂Cl₂], the two chloro ligands are adopting the *cis* positions around the Mn centre (*cis-cis-trans trans-trans-trans* isomer). It is the

first time that a *cis* orientation of the (1,2,3-triazol-4-yl)pyridine ligands and the halogen atoms has been found for an octahedral Mn(II), Fe(II), Co(II) or Ni(II) complex containing two bidentate (1,2,3-triazol-4-yl)pyridine ligands and two halogen atoms. DFT results support experimental measurements, that the metal(II) complexes are high spin and that the *cis-cis-trans* and the *trans-trans-trans* isomers, with the pyridyl groups *trans* to each other, are the lowest in energy.

Supplementary material

Optimized coordinates of the DFT calculations, IR and MS spectra, and additional crystallographic data are given in the Supporting Information.

Acknowledgements

The National Mass Spectroscopy Centre at the University of Wales, Swansea is thanked for supplying the mass spectrometry data. KT expresses his gratitude to the Iraqi Government for financial support to conduct the research reported in the UK. This work has received support from the South African National Research Foundation and the Central Research Fund of the University of the Free State, Bloemfontein, South Africa. The High Performance Computing facility of the University of the Free State and the Centre for High Performance Computing CHPC of South Africa are gratefully acknowledged for computer time.

References

-
- [1] B. O'Regan and M. Grätzel, *Nature*, 1991, **353**, 737–740.
 - [2] K. Hara and S. Mori, in *Handbook of Photovoltaic Science and Engineering, Second Edition*, 2011, p. 642.
 - [3] M. Grätzel, *J. Photochem. Photobiol. C Photochem. Rev.*, 2003, **4**, 145–153.
 - [4] G. C. Vougioukalakis, A. I. Philippopoulos, T. Stergiopoulos, and P. Falaras, *Coord. Chem. Rev.*, 2010, **255**, 2602–2621.
 - [5] Grätzel M., Chen C Y., Wang M K., Li J Y., Pootrakulchote N., Alibabaei L., Ngocle C H., Decoppet J D., Tsai J H, Gratzel C., Wu C G., Nazeeruddin S M., *ACS Nano.*,3:3103 (2009)
 - [6] A. Hagfeldt, G. Boschloo, L. Sun, L. Kloo, and H. Pettersson, *Chem. Rev.*, 2010, **110**, 6595–663.
 - [7] M. Wang and C. Grätzel, *Energy Environ. Sci.*, 2012, **5**, 9394.
 - [8] A. Yella, H.-W. Lee, H. N. Tsao, C. Yi, A. K. Chandiran, M. K. Nazeeruddin, E. W.-G. Diau, C.-Y. Yeh, S. M. Zakeeruddin, and M. Grätzel, *Science*, 2011, **334**, 629–34

-
- [9] J.-H. Yum, E. Baranoff, F. Kessler, T. Moehl, S. Ahmad, T. Bessho, A. Marchioro, E. Ghadiri, J.-E. Moser, C. Yi, M. K. Nazeeruddin, and M. Grätzel, *Nat. Commun.*, 2012, **3**, 631.
- [10] S. Powar, T. Daeneke, M. T. Ma, D. Fu, N. W. Duffy, G. Götz, M. Weidelener, A. Mishra, P. Bäuerle, L. Spiccia, and U. Bach, *Angew. Chemie Int. Ed.*, 2013, **52**, 602–5.
- [11] J. Conradie, M.M. Conradie, K. Tawfiq, M. Al-Jeboori and J.H. Potgieter, Synthesis and characterisation of some novel Fe - 1,2,3-triazole-PYTA (pyridyl group containing) compounds for potential application in dye solar cell and anti-cancer compounds, submitted.
- [12] Kinaan M. Tawfiq, Gary J. Miller, Mohamad J. Al-Jeboori, Paul S. Fennell, Simon J. Coles, Graham J. Tizzard, Claire Wilson and Herman Potgieter, Comparison of the structural motifs and packing arrangements of six novel derivatives and one polymorph of 2-(1-phenyl-1H-1,2,3-triazol-4-yl)pyridine, *Acta Cryst. B*, 2014, **70**, 379–389, doi:10.1107/S2052520614001152

Reference 12 and 13 the same

- [13] Kinaan M. Tawfiq, Gary J. Miller, Mohamad J. Al-Jeboori, Paul S. Fennell, Simon J. Coles, Graham J. Tizzard, Claire Wilson and Herman Potgieter, Comparison of the structural motifs and packing arrangements of six novel derivatives and one polymorph of 2-(1-phenyl-1H-1,2,3-triazol-4-yl)pyridine, *Acta Cryst.* (2014). B70, 379–389, doi:10.1107/S2052520614001152
- [14] Alonso, F., Moglie, Y., Radivoy, G. & Yus, M., *Org. & Biomol. Chem.* **9**, 6385 (2011)
- [15] Park, I. S., Kwon, M. S., Kim, Y., Lee, J. S. & Park, J., *Org. Lett.* **10**, 497-500 (2008).
- [16] Park, H., *Pharmaceutical Patent Analyst.* **3**, 491-498 (2014).
- [17] Crowley, J. D., Bandeen, P. H. & Hanton, L. R., *Polyhedron.* **29**, 70-83 (2010).
- [18] Bain G.A., Berry J.F., *J. Chem. Educ.*, **85**:532(2008)
- [19] Palatinus, L. & Chapuis, G. (2007). *J. Appl. Cryst.* **40**, 786-790
- [20] Rigaku Corporation, CrystalClear-SM Expert 2.0 r13, (2011)
- [21] Dolomanov, O. V., Bourhis, L. J., Gildea, R. J., Howard, J. A. K. & Puschmann, H., *J Appl Cryst.* **42**, 339-341 (2009).
- [22] Sheldrick, G. M., *Acta Cryst Sect A.* **64**, 112-122 (2007).
- [23] Macrae, C F., Bruno I J., Chisholm J A., Edgington P R., McCabe P., Pidcock E., Rodriguez-Monge L., Taylor R., van de Streek J., Wood P.A., *J. Appl. Cryst.*, **41**:466(2008)
- [24] Gaussian 09, Revision D.01, Frisch, M. J.; Trucks, G. W.; Schlegel, H. B.; Scuseria, G. E.; Robb, M. A.; Cheeseman, J. R.; Scalmani, G.; Barone, V.; Mennucci, B.; Petersson, G. A.; Nakatsuji, H.; Caricato, M.; Li, X.; Hratchian, H. P.; Izmaylov, A. F.; Bloino, J.; Zheng, G.; Sonnenberg, J. L.; Hada, M.; Ehara, M.; Toyota, K.; Fukuda, R.; Hasegawa, J.; Ishida, M.; Nakajima, T.; Honda, Y.; Kitao, O.; Nakai, H.; Vreven, T.; Montgomery, J. A., Jr.; Peralta, J. E.; Ogliaro, F.; Bearpark, M.; Heyd, J. J.; Brothers, E.; Kudin, K. N.; Staroverov, V. N.; Kobayashi, R.; Normand, J.; Raghavachari, K.; Rendell, A.; Burant, J. C.; Iyengar, S. S.; Tomasi, J.; Cossi, M.; Rega, N.; Millam, J. M.; Klene, M.; Knox, J. E.; Cross, J. B.; Bakken, V.; Adamo, C.; Jaramillo, J.; Gomperts, R.; Stratmann, R. E.; Yazyev, O.; Austin, A. J.; Cammi, R.; Pomelli, C.; Ochterski, J. W.; Martin, R. L.; Morokuma, K.; Zakrzewski, V. G.; Voth, G. A.; Salvador, P.; Dannenberg, J. J.; Dapprich, S.; Daniels, A. D.; Farkas, Ö.; Foresman, J. B.; Ortiz, J. V.; Cioslowski, J.; Fox, D. J. Gaussian, Inc., Wallingford CT, 2009.
- [25] <http://www.chemcraftprog.com/>
- [26] Jiang L., Wang Zh., Bai Sh.Q., Andy Hor T.S., *Dalton Trans.*, **42**:9437(2013)
- [27] Vellas S K., Lewis J E M., Shankar M., Sagatova A., Tyndall J D A., Monk B. C., Fitchett Ch M., Hanton L R., Crowley J D., *Molecules.*, **18**:6383(2013)
- [28] Lever A B P., *Inorganic Electronic Spectroscopy.*, 2nd edition., Elsevier, New York, p.249 (1986)
- [29] Mahmoud W H., Mohamed G G., El-Dessouky M M I., *Spectrochim. Acta. Part A*, **122**:598(2014)
- [30] Refata M S., El-Metwaly N M., *Spectrochim. Acta. Part A.*, **92**:336(2012)

-
- [³¹] Sowjanya G., Reddy N C G., Reddy S L., Reddy B J., Frost R L., *Spectrochim. Acta Part A.*, **71**:751(2008)
- [³²] Malik S., Ghosh S., Mitu L., *J. Serb. Chem. Soc.*, **76**:1387(2011)
- [³³] Spinu C., Pleniceanu M., Tigae C., *J. Serb. Chem. Soc.*, **73**:415(2008)
- [³⁴] Modi C.K., *Spectrochim. Acta Part A.*, **71**:1741(2009)
- [³⁵] Raman N., Sobha S., Thamaraiichelvan A., *Spectrochim. Acta Part A.*, **78**: 888(2011)
- [³⁶] Revanasiddappa H D., Kumar L S., Prasad K S., Vijay B., Jayalalshmi B., *Chem. Sci. J.*, CSJ-**28**, 1, (2011)
- [³⁷] Gonzalez E., Witchel A R., Reber C., *Coord. Chem. Rev.*, **251**: 351(2007)
- [³⁸] Chandra S., Sharma A. K., *Spectrochim. Acta. Part A.*, **72**:851(2009)
- [³⁹] Al-Jeboori M J., Al-Dujaili., Al-Janabi A H., *Transition. Met. Chem.* **34**: 109(2009)
- [⁴⁰] Tong Y Z., Wang Q., Si M., Qi J., Yan S., Yang G M., Cheng P., Liao D Z., *Polyhedron*, **30**:3151(2011)
- [⁴¹] Cambridge Structural Database (CSD), Version 5.38, May 2017 update.
- [⁴²] Schweinfurth D., Su C Y., Wei S C., Braunsteind P., Sarkar B, Nickel complexes with “click”-derived pyridyl-triazole ligands: weak intermolecular interactions and catalytic ethylene oligomerisation, *Dalton Trans.*, 2012,41, 12984-12990, DOI: 10.1039/C2DT31805A]
- [⁴³] Cambridge Structural Database (CSD), Version 5.38, May 2017 update.
- [⁴⁴] Dey R., Ghoshal D., *Polyhedron*, **34**:24(2012)
- [⁴⁵] Li Y, Zou W Q, Wu M F, Lin J.D, Zheng F K, Liu Z F, Wang S H, Guoa G C., Huang J S., *Cryst. Eng. Comm.* **13**:3868(2011)
- [⁴⁶] Hao E, Wang Z, Jiao L., Wang S., *Dalton Trans.*, **39**:2660(2010)
- [⁴⁷] Hou H., Meng X., Song Y., Fan Y., Zhu Y., Lu H., Du C., Shao W., *Inorg. Chem.*, **41**, 4068:(2002).
- [⁴⁸] Kovács A., Varga Z., *Coord. Chem. Rev.*, **250**:710(2006)
- [⁴⁹] Brammer L., Bruton E.A., Sherwood P., *Cryst. Growth Des.* **1**:277(2001)
- [⁵⁰] Steiner. T., *Angew. Chem. Int. Ed.*, **41**:48(2002)
- [⁵¹] Jeffrey G A., *An Introduction to Hydrogen Bonding*, Oxford University Press, Oxford(1997)
- [⁵²] Aakeroy C B., Evans T A., Seddon K R. Palinko I., *New J. Chem.*, **23**: 145(1999)
- [⁵³] Yang Y., Du P., Yang J., Kan W Q., Ma J F., *Cryst. Eng. Commun.* **15**: 4357(2013)
- [⁵⁴] Janiak C., *J. Chem. Soc., Dalton Trans.*, 3885(2000)
- [⁵⁵] Košmrlj J G., Urankar D., Pevec A., Turel I., *Cryst. Growth Des.* **10**:4920(2010)
- [⁵⁶] Bratsos I., Urankar D., Zangrando E., Kalou P., Kosmrlj G., Alessio J E., Turel I., *Dalton Trans.*, **40**:5188(2011)